Collana di Aggiornamenti

NUMERO 12

CIAMMAICHELLA
DE PAOLA
MAIDA
ULISSI
PETRECCA
MARZANO
FANFARILLO
PIGNATA
PUGLISI
ALA
DI CASTRI

INFERIOR VENA CAVA ANOMALIES: CASES REPORT

Collana di Aggiornamenti della SCUOLA MEDICA OSPEDALIERA
B.go S. Spirito, 3 ~ 00193 Roma~Tel. 06/688.02.626 - 683.52.411
www.smorrl.it

Collana di Aggiornamenti

INFERIOR VENA CAVA ANOMALIES: CASES REPORT

Ciammaichella Maurizio Maria, De Paola Giuseppe, Maida Rosa, Ulissi Alessandra, Petrecca Isabella, Marzano Maria Adelaide, Fanfarillo Francesca, Pignata Daniele, Puglisi Lucia, Ala Angelica, Di Castri Carla

Collana di Aggiornamenti della Scuola Medica Ospedaliera
Segreteria: B.go S. Spirito, 3 - 00193 Roma Tel. 06.6880.2626 - 06.6835.2411 Fax 06.6880.6712
N° 12 ~ Supplemento al n° 41 Gennaio-Marzo 2019 del Trimestrale
S.M.O. - Bollettino della Scuola Medica Ospedaliera
Autorizzazione Tribunale di Roma n. 86/95 del 18/02/95

INDICE

INFERIOR VENA CAVA ANOMALIES: CASES REPORT.

AUTORI

Ciammaichella Maurizio Maria
Dirigente Medico, Responsabile Incarico Professionale A.S.1 "Gestione della Trombosi Venosa Profonda ed Embolia Polmonare nell'Area dell'Emergenza"
UOC Medicina d'Urgenza
Direttore: Dott. ssa R. Maida
A.O. S. Giovanni Addolorata, Roma

De Paola Giuseppe
Dirigente Medico, UOC Medicina d'Urgenza
Direttore: Dott. ssa R. Maida
A.O. S. Giovanni Addolorata, Roma

Maida Rosa
Direttore, UOC Medicina d'Urgenza
A.O. S. Giovanni Addolorata, Roma

Ulissi Alessandra
Dirigente Medico, Responsabile I. P. A. S. "Gestione post-dimissione dei pazienti in terapia con NAO"
UOC Medicina d'Urgenza
Direttore: Dott. ssa R. Maida
A.O. S. Giovanni Addolorata, Roma

Petrecca Isabella
Dirigente Medico, Responsabile U.A.S. "Appropriatezza dei Ricoveri e Qualità dell'Assistenza"
UOC Medicina d'Urgenza
Direttore: Dott. ssa R. Maida
A.O. S. Giovanni Addolorata, Roma

Marzano Maria Adelaide
Dirigente Medico, UOC Medicina d'Urgenza
Direttore: Dott. ssa R. Maida
A.O. S. Giovanni Addolorata, Roma

Fanfarillo Francesca
Dirigente Medico, UOC Medicina d'Urgenza
Direttore: Dott. ssa R. Maida
A.O. S. Giovanni Addolorata, Roma

Pignata Daniele
Dirigente Medico, UOC Medicina d'Urgenza
Direttore: Dott. ssa R. Maida
A.O. S. Giovanni Addolorata, Roma

Puglisi Lucia
Dirigente Medico, UOC Medicina d'Urgenza
Direttore: Dott. ssa R. Maida
A.O. S. Giovanni Addolorata, Roma

Ala Angelica
Dirigente Medico, UOC Medicina d'Urgenza
Direttore: Dott. ssa R. Maida
A.O. S. Giovanni Addolorata, Roma

Di Castri Carla
Dirigente Medico, UOC Medicina d'Urgenza
Direttore: Dott. ssa R. Maida
A.O. S. Giovanni Addolorata, Roma

INTRODUCTION

A broad spectrum of congenital anomalies and pathologic conditions can affect the inferior vena cava (IVC). Most congenital anomalies are asymptomatic; consequently, an awareness of their existence and imaging appearances is necessary to avoid misinterpretation.

Imaging also plays a central role in the diagnosis of Budd-Chiari syndrome secondary to membranous obstruction of the intrahepatic IVC. Primary malignancy of the IVC is far less common than intracaval extension of malignant tumors arising in adjacent organs, and imaging can accurately help determine the presence and extent of tumor thrombus, information that is crucial for surgical planning. However, the radiologist should be aware that artifactual filling defects at computed tomography and magnetic resonance imaging can mimic true thrombus in the IVC and must be able to differentiate true from pseudo filling defects.

Other imaging findings such as flat IVC and early enhancement of the IVC are useful in limiting the differential diagnosis.

Familiarity with the imaging features of the various congenital and pathologic entities that can affect the IVC is paramount for early diagnosis and management. Imaging plays a crucial role in the diagnosis and management of diverse conditions that affect the inferior vena cava (IVC).

ltrasonography (US), including color Doppler flow imaging, is a useful modality for initial evaluation. It complements computed tomography (CT) and magnetic resonance (MR) imaging in the diagnosis of Budd-Chiari syndrome (BCS) and in the depiction of tumor thrombus and its cranial extent, and helps differentiate artifactual filling defects from true thrombus. However, US

is operator dependent, and visualization of the IVC (especially the infrahepatic portion) may be hampered due to bowel gas or obesity. CT and MR imaging are essential for staging and treatment planning.

There is no standard CT protocol for imaging of the IVC. The IVC is typically evaluated in the portal venous phase (60–70 seconds after the injection of 100–150 mL of nonionic contrast material at a rate of 3–5 mL/sec), and dynamic multiphasic imaging is performed only if otherwise indicated (eg, in renal cell carcinoma). In the portal venous phase, there is denser contrast material in the renal and suprarenal IVC than in the infrarenal portion due to venous return from the kidneys.

This fact should be borne in mind to avoid pitfalls (discussed later), and, in cases of a possible filling defect, delayed imaging should be performed. The isotropic volume data sets that are possible with the latest-generation multi detector CT scanners allow superior-quality multiplanar reformation, which is useful in delineating IVC disease.

MR imaging is the most reliable technique for depicting the presence and extent of tumor thrombus, although limited availability and cost considerations prohibit its routine use. Three-dimensional breath-hold T1-weighted MR imaging performed after the intravenous administration of contrast material and balanced steadystate free precession are the most robust MR imaging sequences for imaging of the IVC.

In this article, we review the imaging features of various congenital anomalies of the IVC, including left IVC, double IVC, retrocaval ureter, absence of the infrarenal IVC, retroaortic and circumaortic left renal vein, interruption of the IVC with azygous or hemiazygous continuation, and portocaval shunt.

In addition, we discuss and illustrate membranous obstruction of the intrahepatic IVC, bland thrombus and intracaval tumors, the appearance of the IVC in trauma patients, and conditions resulting in early IVC enhancement. We also discuss pitfalls in imaging of the IVC.

CASES REPORT

A basic knowledge of IVC embryogenesis is essential for understanding the anomalies of the IVC. A detailed review of IVC formation is beyond the scope of this article, but the interested reader can refer to an excellent review by Phillips (1). Briefly, during the 4th week of fetal life, paired posterior cardinal veins drain the caudal portion of the embryo. These veins are progressively replaced, first by the subcardinal veins and later by the supracardinal veins, which together form the subhepatic IVC (2). As their names imply, the subcardinal veins are ventromedial and the supracardinal veins dorsomedial to the posterior cardinal veins. The right subcardinal vein forms the suprarenal segment of the IVC, and the right supracardinal vein forms the infrarenal segment. Anastomotic channels between the supracardinal and subcardinal veins form the intervening renal segment of the IVC. Cranially, the subcardinal vein (suprarenal IVC) forms an anastomosis with the hepatic segment, which is derived from the right vitelline vein. Caudally, the infrarenal IVC (right supracardinal vein) forms an anastomosis with the iliac veins, which are derived from the persistent posterior cardinal veins (**FIG. 1**) (2). IVC anomalies reflect an abnormal regression or persistence of the various embryonic veins (3). Although most anomalies are symptomatic (4) and are encountered incidentally, their correct identification is useful in the planning of vascular interventions and prevents their being mistaken for disease.

CASE 1

Left IVC has a prevalence of 0.2% – 0.5% (1) and represents a persistent left supracardinal vein. The right supracardinal vein regresses in these cases, resulting in a mirror image variant. A leftsided IVC typically joins the left renal vein, and together they course anterior to the aorta to join the normal (right-sided) IVC (**FIG. 2**). A left-sided IVC per se is of no clinical importance. However, it may be mistaken for left paraaortic adenopathy (5), complicate surgical repair of an aortic neurysm (6), and cause difficulty in placing an infrarenal IVC filter with a transjugular approach (3).

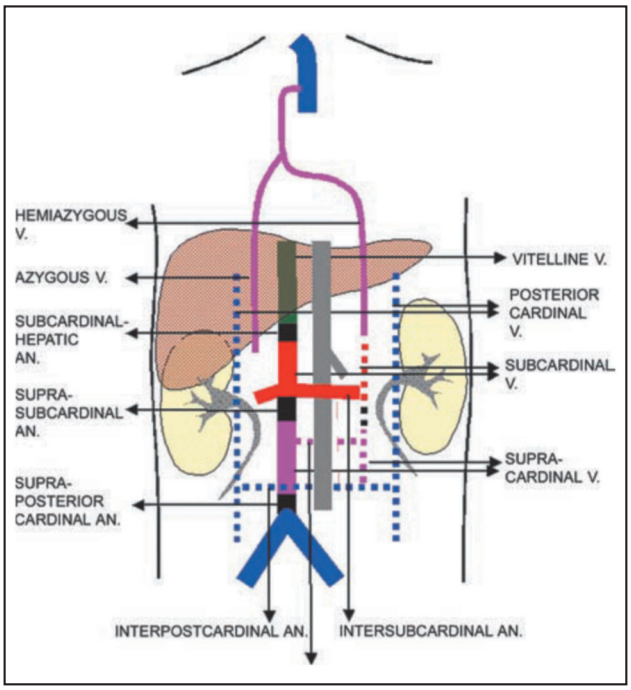

FIGURE 1

Drawing illustrates the embryologic development of the IVC. Three pairs of veins - the posterior cardinal (blue), subcardinal (vertical red), and supracardinal (purple) veins - develop in succession on either side of the aorta (gray). Portions of these venous channels regress (dashed colored lines), whereas others persist (solid colored lines) to form the infrahepatic IVC. The right subcardinal vein forms the suprarenal segment of the IVC, and the right supracardinal vein forms the infrarenal segment. The hepatic segment is derived from the vitelline vein (green). Anastomotic channels (black) connect the various segments of the IVC. An intersubcardinal anastomosis that passes anterior to the aorta forms the left renal vein (horizontal red line), whereas intersupracardinal and interposterior cardinal anastomoses normally regress. The supracardinal veins continue as the azygous and hemiazygous veins; the iliac veins are derived from the persistent posterior cardinal veins. *AN* = anastomosis, *V* = vein.

FIGURE 2

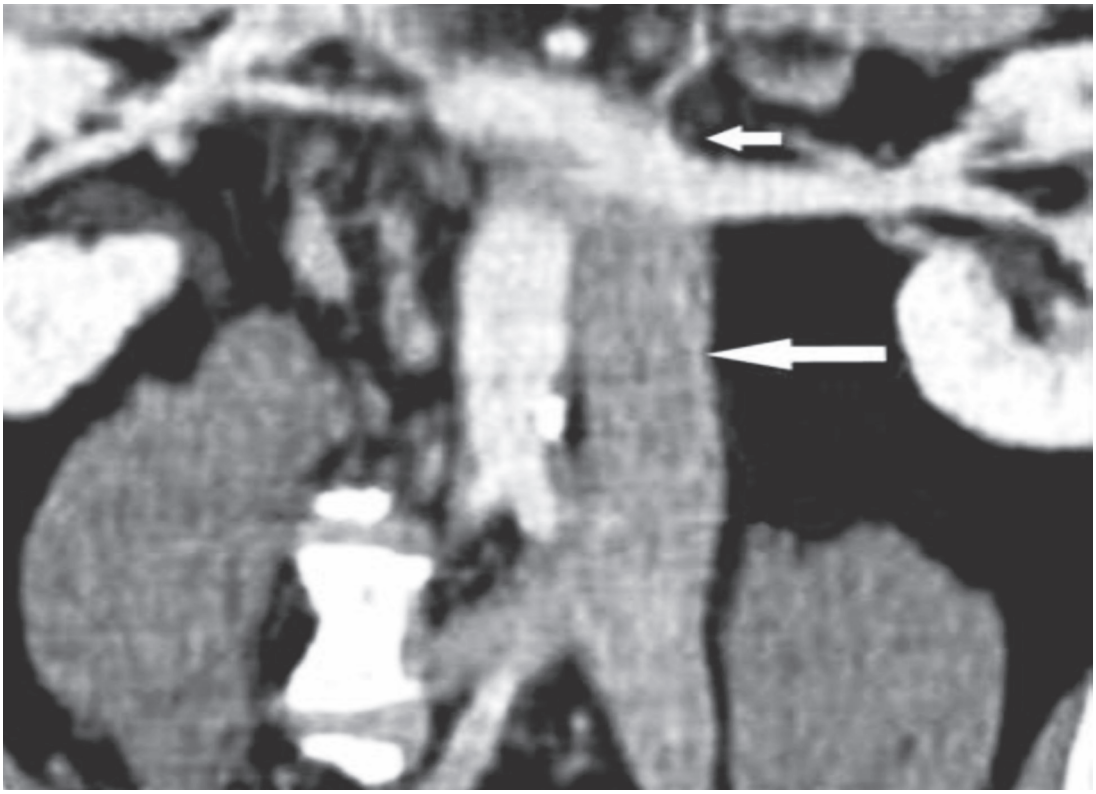

Left IVC. Coronal curved reformatted CT image shows a left-sided IVC (large arrow) joining the left renal vein (small arrow), which unites with the right renal vein to form a normal right-sided suprarenal IVC.

CASE 2

Double (right and left) IVC has a prevalence of 1%–3% and results from persistence of both the right and left supracardinal veins (1). Typically, the left IVC drains into the left renal vein, which then joins the right IVC (**FIG. 3**). There may be significant discrepancy in the size of the two veins. Double IVC has clinical implications that are similar to those of left IVC and may be istaken for adenopathy, especially if contrast enhancement of the vein is poor due to technical reasons or thrombosis (7). Double IVC should be suspected in cases of recurrent episodes of pulmonary embolism despite placement of an IVC filter (1). There are only a few reports describing the technique of filter placement in patients with venous thrombosis and double IVC. The options vary from placing a single filter in the common suprarenal IVC (8), to infrarenal filter placement in the IVC on each side (9), to steel coil embolization of the smaller IVC coupled with filter placement in the contralateral IVC (10).

FIGURE 3

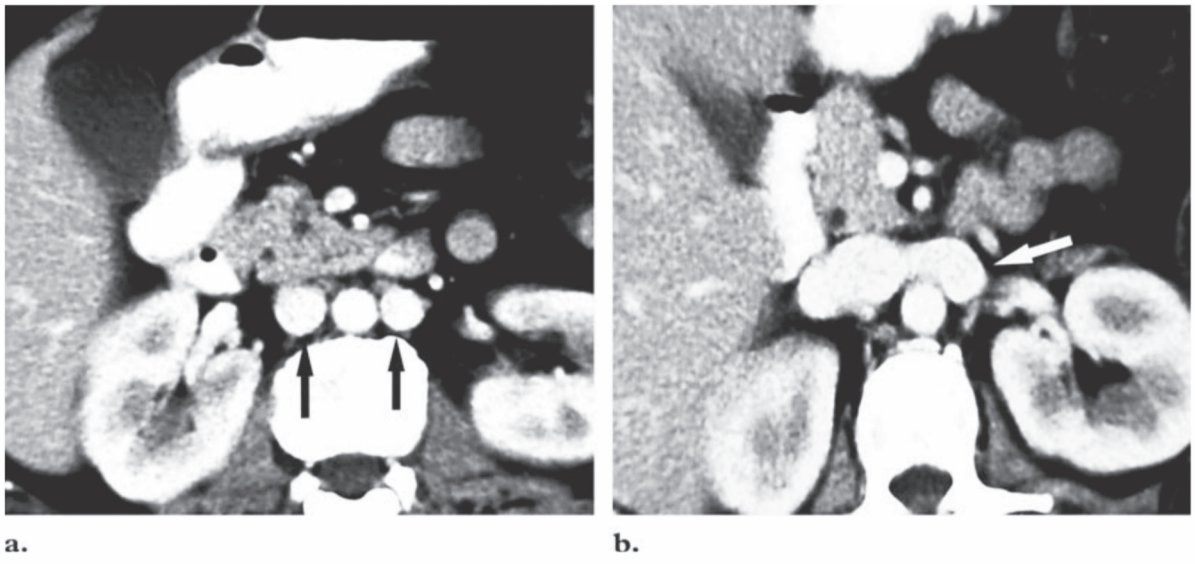

Double IVC. **(a)** Contrast material–enhanced caudocranial CT scan shows right and left infrarenal IVCs (arrows). **(b)** Contrast-enhanced caudocranial CT scan shows the left IVC opening into the left renal vein (arrow), which crosses anterior to the aorta to form a single rightsided suprarenal IVC.

CASE 3

Retrocaval ureter is one of the few congenital anomalies of the IVC that can be symptomatic (4). Unlike other congenital ureteral obstructions, this embryologic defect lies in the developing vena cava rather than the ureter. In this condition, the infrarenal IVC develops from the right posterior cardinal vein, which lies anterior and lateral to the ureter - unlike the normal situation, in which the IVC is formed by the right supracardinal vein, located posterior and medial to the ureter. As a result, part of the right ureter becomes trapped posterior and medial to the IVC. En route, the ureter can undergo significant compression, resulting in hydronephrosis or recurrent urinary tract infections (3). The diagnosis can be made at intravenous urography, which reveals the abnormal course of the proximal ureter as it projects over or medial to the lumbar pedicles on frontal images with proximal hydronephrosis, resulting in the characteristic “fish hook” or “reverse J” appearance (11). CT elegantly depicts the abnormal course of the ureter. Treatment consists of surgical relocation of the ureter anterior to the IVC (1).

CASE 4

Complete absence of the infrarenal IVC with preservation of the suprarenal segment is an extremely rare anomaly (**FIG. 4**) (12). This condition may be a sequela of intrauterine or perinatal thrombosis of the IVC and not truly embryologic in origin (13,14). Affected patients are prone to develop deep venous thrombosis (15) and chronic venous insufficiency (14,16). Lower-extremity venous return in these patients occurs via the ascending lumbar veins, which drain into the azygous-hemiazygous system. Enlarged collateral vessels may simulate a paraspinal mass (13).

FIGURE 4

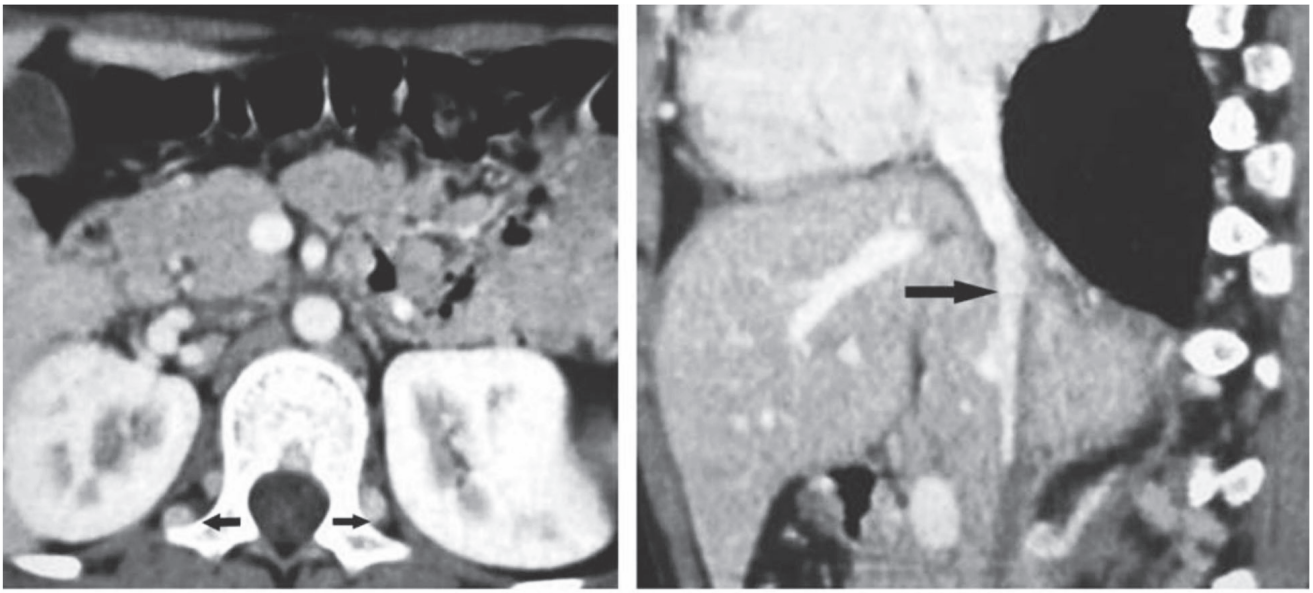

IVC agenesis. Axial contrast-enhanced CT scan (**a**) and sagittal curved reformatted CT image (**b**) show absence of the infrarenal IVC. Note the prominent ascending lumbar veins (arrows in **a**) and the patent suprarenal IVC (arrow in **b**).

CASE 5

Anomalies of the renal segment of the IVC include variants of the left renal vein. Normally, the left renal vein is derived from the intersubcardinal anastomoses, which course anterior to the aorta (2). The left renal vein is retroaortic in 1.7% – 3.4% of individuals (**FIG. 5**) and occurs when the vein derives from the intersupracardinal veins, which lie posterior to the aorta.

Persistence of both the intersupracardinal and intersubcardinal veins results in a circumaortic venous ring, with one vein coursing anterior and the other posterior to the aorta (prevalence, 2.4% – 8.7%) (**FIG. 6**) (4). The posteriorly located renal vein is caudad with respect to the preaortic vein (4).

These renal vein anomalies assume significante in the preoperative planning of nephrectomy and can be misdiagnosed as adenopathy (3). On rare occasions, compression of the renal vein as it courses posterior to the aorta (nutcracker phenomenon) can result in periureteric varices, hypertension, and hematuria (**FIG. 5**) (17).

FIGURE 5

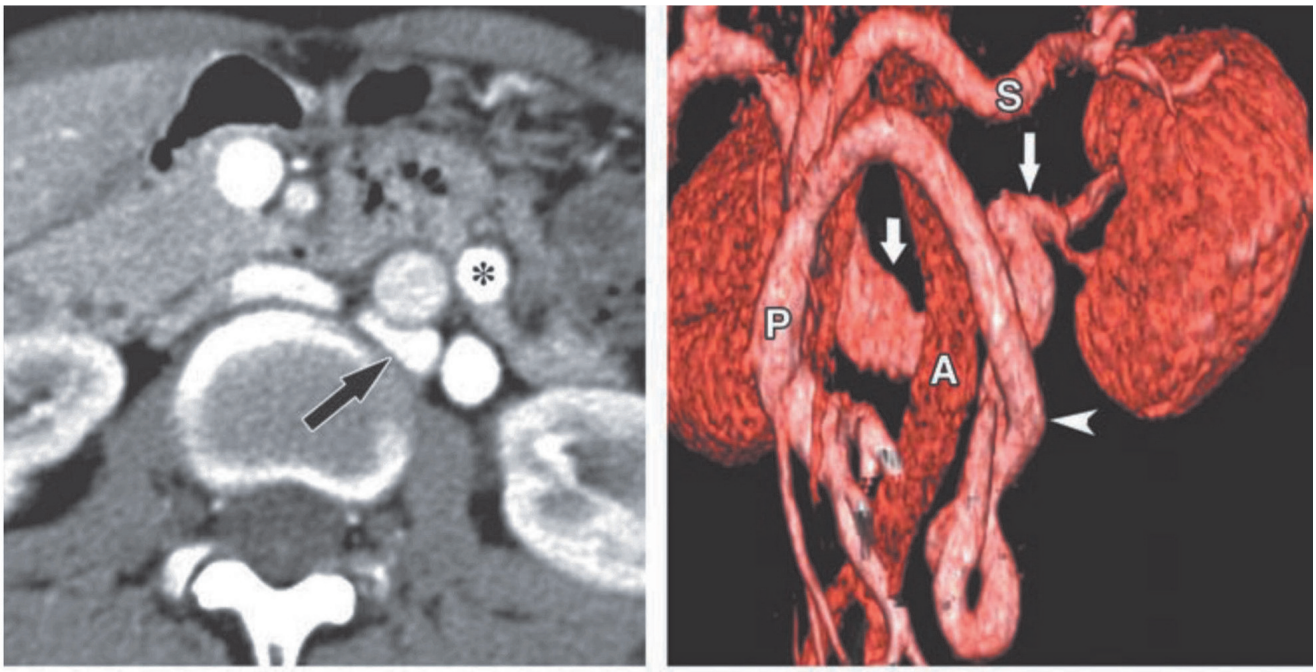

a. **b.**

Retroaortic left renal vein causing hypertension and hematuria in a 45-year-old woman. **(a)** Contrast-enhanced CT scan shows compression of the left renal vein as it corse posterior to the aorta (arrow) ("nutcracker phenomenon"), along with prominent periureteric collateral vessels **(*)**. **(b)** Volume-rendered image (anterolateral view) shows the left renal vein (arrows) coursing posterior to the aorta **(A)**, with a prominent periureteric collateral vessel (arrowhead) draining into the portosplenic confluence. **P** = portal vein, **S** = splenic vein.

FIGURE 6

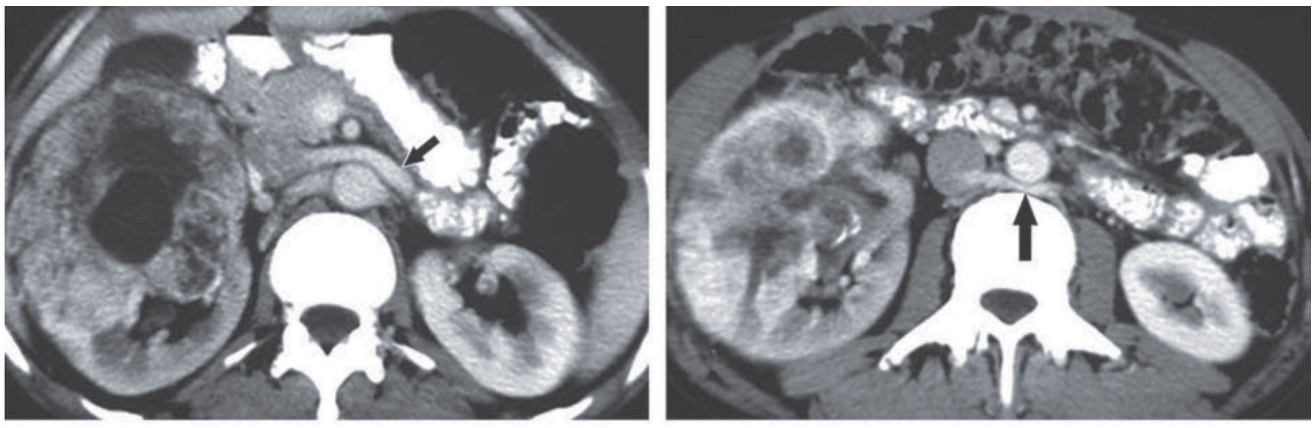

a. **b.**

Circumaortic left renal vein in a 47-year-old patient with right renal cell carcinoma. Contrast-enhanced craniocaudal CT scans show the left renal vein coursing anterior (arrow in **a**) and posterior (arrow in **b**) to the aorta.

FIGURE 7

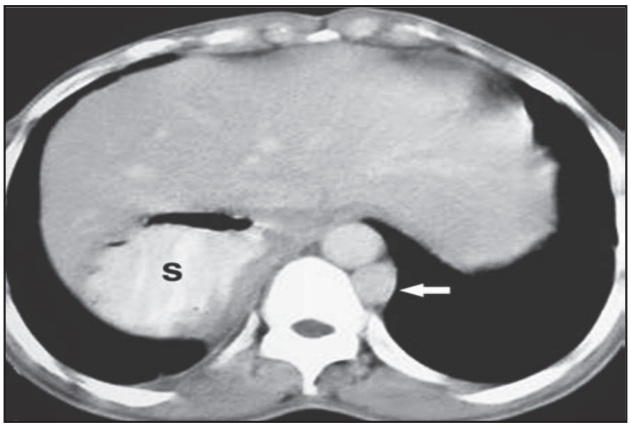

IVC interruption with hemiazygous continuation. Contrast-enhanced CT scan shows hemiazygous continuation (arrow) of a left-sided IVC (not shown). Associated findings of a midline liver and a portion of the stomach **(S)** in the right upper quadrant are suggestive of situs ambiguous.

FIGURE 8

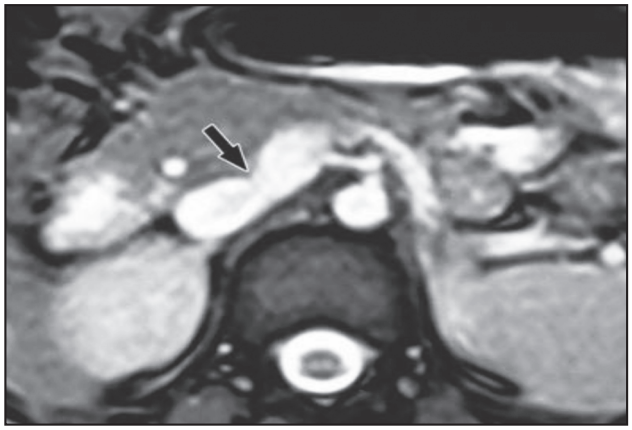

Portocaval shunt in a 6-year-old girl with elevated serum ammonia levels. Axial balanced steady state (true fast imaging with steady state precession [FISP]) MR image shows complete end-to-side fistulous communication (arrow) between the portal vein and the IVC.

CASE 6

Interruption of the IVC with azygous or hemiazygous continuation results from failed formation of the right subcardinal-hepatic anastomosis, with consequent atrophy of the subcardinal vein (suprarenal IVC) (3). The infrarenal IVC continues as the azygous vein and, in cases of left IVC, as the hemiazygous vein (**FIG. 7**) (4). Associated situs anomalies are present in many of these cases. It is important not to misinterpret the enlarged azygous or hemiazygous veins as adenopathy (18). Preoperative knowledge of this anomaly is important in planning cardiopulmonary bypass surgery and can help avoid difficulties in cardiac catheterization (19).

CASE 7

Congenital extrahepatic portocaval shunt is a rare anomaly (20). Two types have been descrive (21): Type I shunt is a complete end-to-side shunt between the portal vein and the IVC, with the main portal vein distal to the shunt being absent (**FIG. 8**); type II shunt is a partial side-to-side shunt between the portal vein and the IVC. Both types result in metabolic derangements and often have associated cardiac, renal, skeletal, or other anomalies (20). Regenerative benign liver nodules are commonly seen in these patients and have been attributed to hepatic ischemia with a compensatory increase in hepatic arterial flow (22). Liver transplantation is the only definitive treatment for type I shunt, whereas treatment of patients with type II shunt is simpler (ligation or coil embolization of the shunt vessel) (20). Congenital intrahepatic shunts between the portal vein branches and the IVC have also been described and can cause hepatic encephalopathy (23).

CASE 8

Membranous obstruction of the intrahepatic IVC accounts for most cases of primary BCS in India, Nepal, South Africa, Japan, China, and Korea (24). It is typically a disease of adulthood with an insidious onset and a chronic course that eventually leads to congestive

cirrhosis (24,25). In contrast, in most Western nations, BCS results from hepatic venous thrombosis due to an nderlying prothrombotic state, has an acute onset, and is often fatal. The cause of membranous obstruction of the intrahepatic IVC remains unclear in the majority of cases; however, evidence is mounting that it is a sequela of IVC thrombosis (26,27). Color Doppler flow US, CT, MR imaging, hepatic enography, and cavography are used in the imaging of IVC obstruction. The imaging appearance of membranous obstruction of the intrahepatic IVC ranges from a short weblike narrowing to a longer segmental occlusion with or without narrowing of the hepatic veins. Intrahepatic venovenous, portocaval, and spider web collateral vessels develop to decompress the liver parenchyma (**FIG. 9**) (28). The inferior (accessory) right hepatic vein (when present) serves as an important draining channel for the intrahepatic collateral vessels (**FIG. 10**).

FIGURE 9

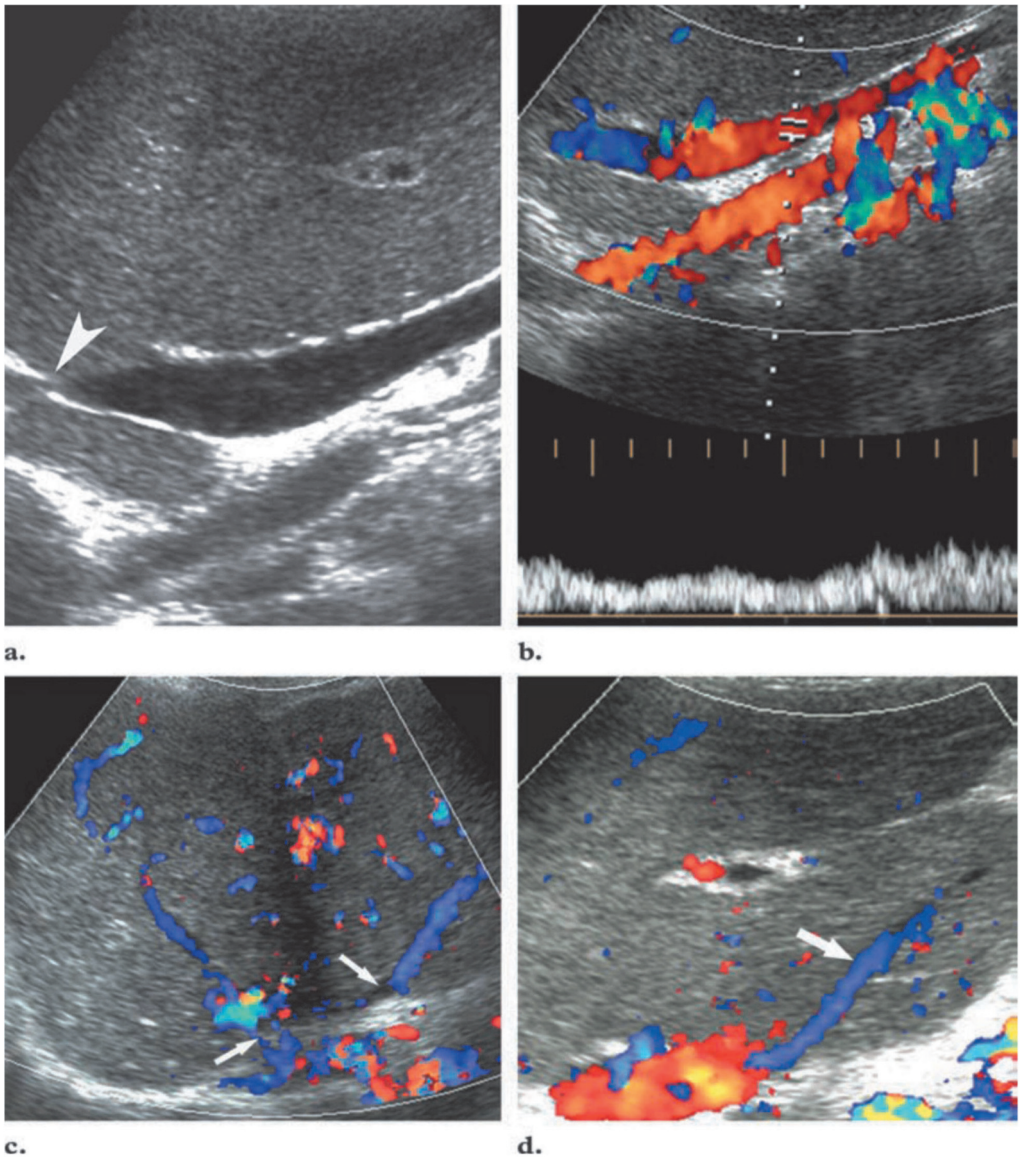

Membranous obstruction of the intrahepatic IVC in a 30-year-old woman who presented with abdominal pain and distention of 3 years duration. **(a)** Sagittal oblique US image shows tapered occlusion of the IVC at the cavoatrial junction (arrowhead). **(b)** Color Doppler US image shows cardiofugal flow in the IVC with loss of transmitted cardiac pulsations. **(c)** Color Doppler US image shows associated ostial narrowing of the hepatic veins (arrows), along with multiple intrahepatic collateral vessels. **(d)** Color Doppler US image shows a hypertrophic caudate lobe, with a prominent caudate vein (arrow) draining into the IVC.

FIGURE 10

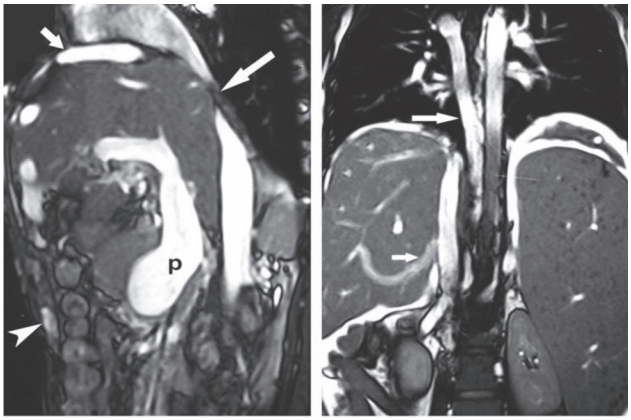

Membranous obstruction of the intrahepatic IVC in a 25-year-old patient who had experienced repeated episodes of hematemesis. Sagittal **(a)** and coronal **(b)** bilance steady-state (true FISP) MR images show segmental occlusion of the IVC at the cavoatrial junction (large arrow in **a**) with enlarged pericardiophrenic veins (small arrow in **a**), anterior abdominal wall collateral vessels (arrowhead in **a**), a dilated inferior (accessory) hepatic vein (small arrow in **b**), and an enlarged azygous vein draining into the superior vena cava (large arrow in **b**). The dilated portal vein **(p)**, ascites, and gross splenomegaly are suggestive of portal hypertension.

FIGURE 11

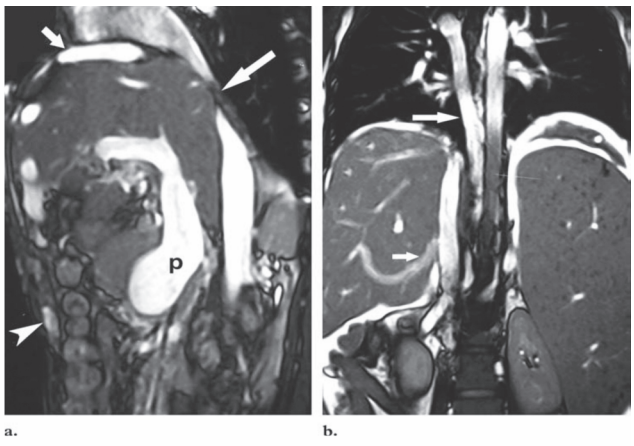

Membranous obstruction of the intrahepatic IVC in a 34-year-old patient with abdominal distention. **(a)** Cavogram shows occlusion of the intrahepatic IVC with retrograde enhancement of the left renal vein (arrow), as well as a large venous pouch **(*)** with faint enhancement of the hemiazygous vein (arrowhead). **(b)** Coronal balanced steady-state (true FISP) MR image shows the large venous pouch (large arrow) and a prominent, tortuous azygous vein (small arrow).

Extrahepatic collateral vessels commonly seen in membranous obstruction of the intrahepatic IVC include the ascending lumbar veins, which drain into the azygous vein on the right side and the hemiazygous vein on the left (**FIG. 10**). Flow may also be directed via the left renalhemiazygous collateral pathway (**FIG. 11**), inferior phrenic-pericardiophrenic collateral vessels, extrahepatic portosystemic collateral vessels, and superficial collateral vessels of the abdominal wall (29). Occasionally, these venous collateral vessels may form a large varix (**FIG. 11**), which can simulate a mass on poorly enhanced images. Because the caudate lobe drains directly into the IVC, it is least affected in BCS and most commonly un-dergoes hypertrophy (80% of cases) (**FIG. 9**) (30). An enlarged caudate vein measuring over 2 mm is seen in 50% of cases and was recently reported to be a specific sign of BCS (**FIG. 9**) (31). Caudate lobe hypertrophy is not specific for BCS; it can also be seen in patients with cirrhosis and extrahepatic portal venous obstruction (32). An enlarged caudate lobe from any cause may also result in a long-segment smooth extrinsic impression on the IVC, which is distinct from the intrinsic narrowing of the cavoatrial junction seen in membranous obstruction of the intrahepatic IVC (**FIG. 12**).

As a result of outflow tract obstruction, portal venous flow becomes sluggish or even reversed, resulting in thrombosis in 10% – 20% of patients (30). In acute BCS, the central regions of the liver, including the caudate lobe and part of the left lobe, enhance normally and appear hyperenhancing relative to the peripheral liver, which shows decreased enhancement. Later, as the contrast medium washes out of the central portion of the liver and accumulates peripherally, the central region appears relatively hypoenhancing (flip-flop pattern of enhancement). In chronic BCS, liver parenchymal enhancement is more variable, being heterogeneous in the early phase and becoming more uniform over time (33). The association between membranous obstruction of the intrahepatic IVC and hepatocellular carcinoma (HCC) is well established as varying greatly between geographic regions: 40% – 48% in South Africa (in the black population) (34,35), 41% in Japan (36), 11% in India, and 4.7% in Nepal (24,37). It is postulated that hepatic congestion causing centrilobular necrosis and perpetual regenerative activity, in conjunction with

an as yet unidentified hepatocarcinogen prevalent in these geographic regions, underlies the development of HCC in these patients (24,25). The diagnosis of HCC in patients with BCS is not straightforward, since these patients are also known to develop regenerative nodules with overlapping imaging features (38,39). Regenerative nodules are observed at pathologic examination in 60% - 80% of patients with BCS (40,41) and are thought to result from a decrease in portal venous flow (42). Because most lesions are small, only a few are identified at imaging (39). They are typically multiple, hyperattenuating at unenhanced CT, hyperintense at T1-weighted MR imaging, iso-or hypointense at T2-weighted MR imaging, and uniformly enhancing in the arterial phase (**FIG. 13**).

FIGURE 12

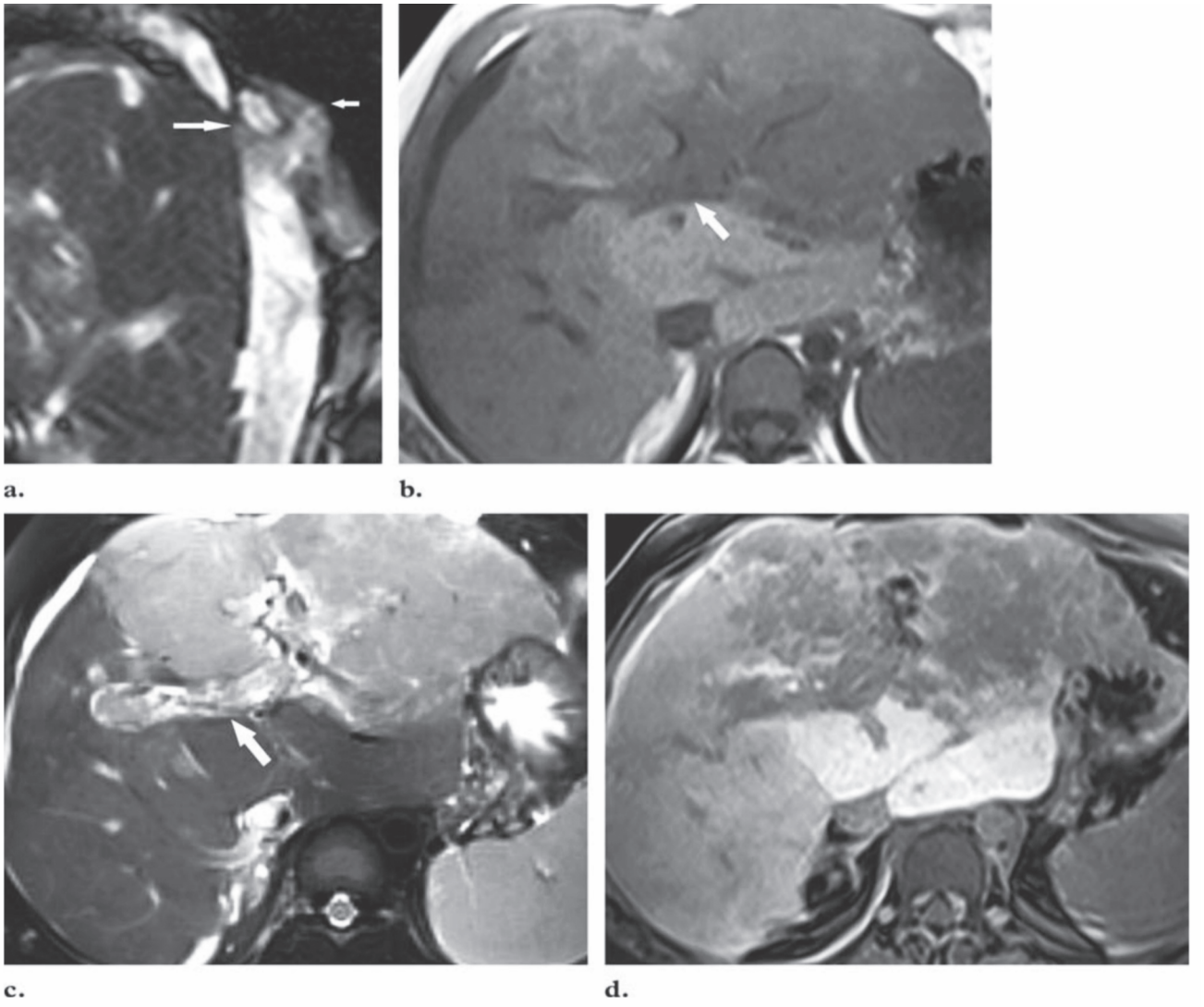

Membranous obstruction of the intrahepatic IVC with HCC in a 55-year-old noncirrhotic woman who presented with abdominal pain and markedly elevated α-fetoprotein levels. **(a)** Sagittal true FISP MR image shows a short weblike narrowing of the IVC (large arrow) with pericardiophrenic collateral vessels (small arrow). The mass was heterogeneously enhancing in the arterial phase. **(b–d)** The mass is hypointense on a T1-weighted MR image **(b)**, is hyperintense on a T2-weighted MR image **(c)**, and does not show Gd- BOPTA uptake on a delayed hepatocyte-specific phase MR image **(d)**. The portal vein flow void is replaced by tumor thrombus (arrow in **b** and **c**).

FIGURE 13

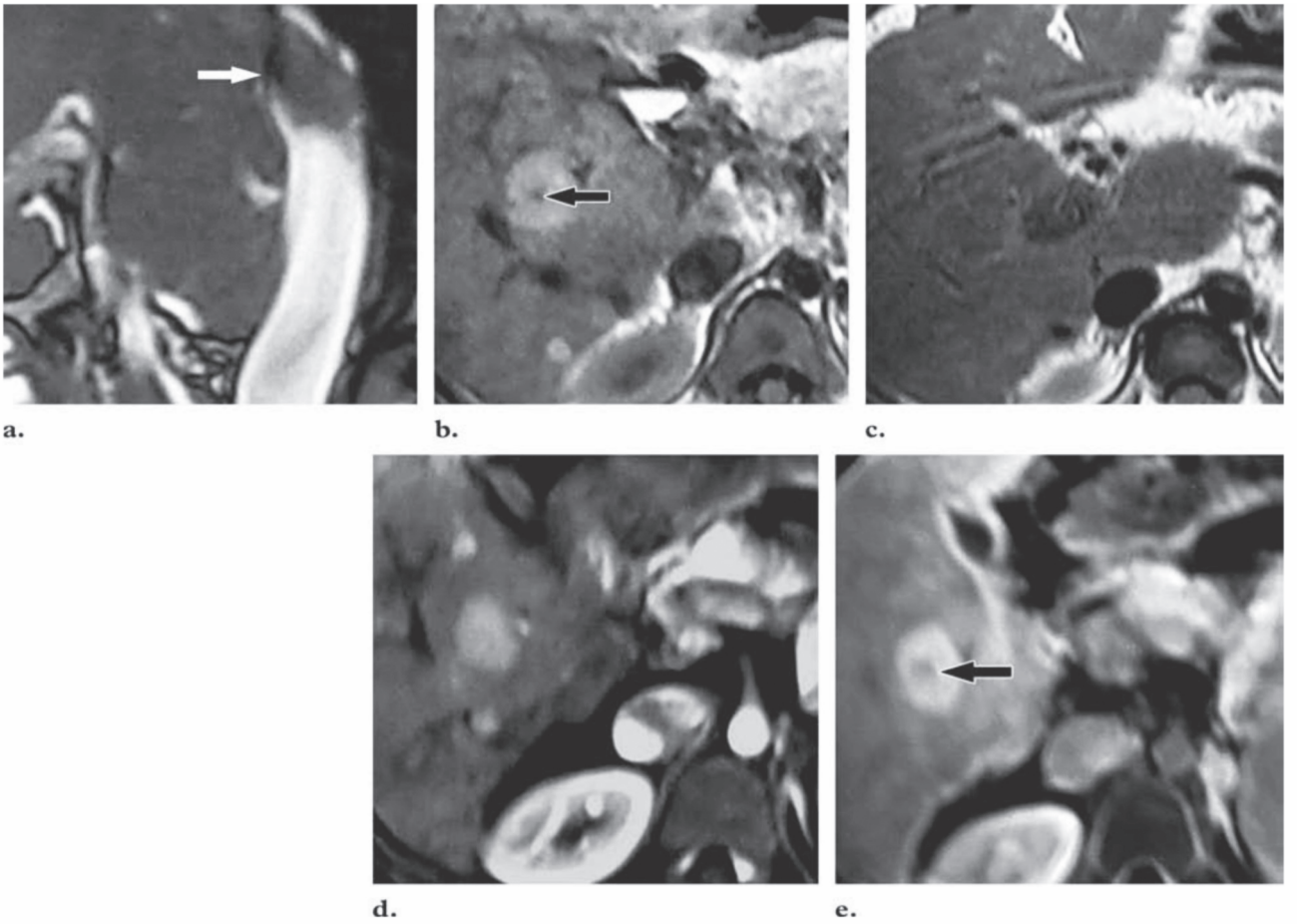

Membranous obstruction of the intrahepatic IVC with regenerative nodules. **(a)** Sagittal true FISP MR image reveals occlusion of the IVC (arrow). **(b–d)** T1-weighted **(b)**, T2-weighted **(c)**, and gadolinium benzyloxypropionic tetraacetate (Gd-BOPTA)–enhanced **(d)** MR images show multiple focal liver lesions, which are hyperintense in **b**, are hypointense in **c**, and show prominent arterial enhancement in **d**. Arrow in **b** indicates a central scar, which is a characteristic feature of benign hepatic nodules. **(e)** MR image shows the uptake and retention of Gd-BOPTA that had been administered 1 hour earlier, a finding that indicates the presence of hepatocytes and delayed clearance of bile. Arrow indicates the central scar.

CASE 9

Bland thrombus, which is the leading cause of IVC obstruction, typically originates in the lower extremities or the pelvis (29). Affected patients often have an underlying predisposing condition such as dehydration, sepsis, localized inflammation, pelvic inflammatory disease, coagulopathy, congestive heart failure, immobility, or trauma (29). Intracaval extension of benign tumors is an extremely rare occurrence that has been reported in renal angiomyolipoma and adrenalpheochromocytoma (43,44). Very rarely, malignant or even benign pheochromocytoma can extend into the IVC. Benign tumor extends via the adrenal veins, whereas malignant pheochromocytoma directly invades the caval wall (44,45). Intravenous leiomyomatosis is a smooth muscle tumor that either arises in the uterine veins or represents intravenous invasion by a uterine fibroma (46 - 48). Although this tumor is usually confined to the pelvic veins, it can have intracaval or even

intracardiac extension. Despite being histologically benign, its potential to result in distant metastases betrays its malignant nature (48). Intravenous leiomyomatosis is strictly confined to females of reproductive age, the majority of whom either harbor uterine leiomyoma or have undergone hysterectomy for this disease entity in the past (46). Tumor thrombus seen at imaging is nonspecific and indistinguishable from primary caval leiomyosarcoma. However, imaging depicts the extent of the tumor, information that is crucial for surgical planning. Leiomyosarcoma is the most common primary malignant tumor of the IVC, most frequently affecting women in the 5th and 6th decades of life (49). Symptomatology and surgical resectability are both dependent on the location of the tumor. The majority arise in the middle (50.8% of cases) or lower (44.2%) third of the IVC (49). Leiomyosarcoma of the upper third of the IVC is rare (4.2% of cases) and is least amenable to surgical resection. The tumor can be completely intraluminal or can have both extra- and intraluminal components (**FIG. 14**) and has a poor prognosis (49). Apart from a primary IVC tumor, leiomyosarcoma arising in the retroperitoneum can secondarily invade the IVC, a peculiar growth pattern not seen in other retroperitoneal sarcomas (50). Contiguous tumor extension directly into the IVC is common in renal cell carcinoma (**FIG. 15**), HCC, adrenocortical carcinoma (**FIG. 16**), and Wilms tumor (**FIG. 17**) (51). Expansion of the vessel lumen and enhancement of the filling defect help differentiate malignant from bland thrombus (29,51). Malignant thrombi in the IVC are often clinically asymptomatic, although occasionally they can result in BCS (51,52) and can embolize into the pulmonary circulation (51). Especially in renal cell carcinoma, tumor thrombi show little tendency to invade the venous wall, allowing complete surgical removal in most cases. In the unlikely event of tumor thrombus infiltrating the venous wall, segmental resection of the IVC becomes essential (53). Unfortunately, involvement of the venous wall is difficult to assess at imaging and is usually diagnosed only at surgical exploration (53).

FIGURE 14

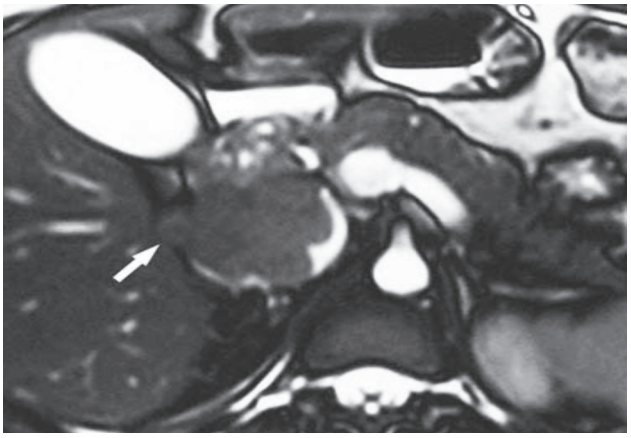

IVC leiomyosarcoma. Axial true FISP MR image shows a predominantly intracaval lobulated mass with a smaller extraluminal component (arrow).

FIGURE 15

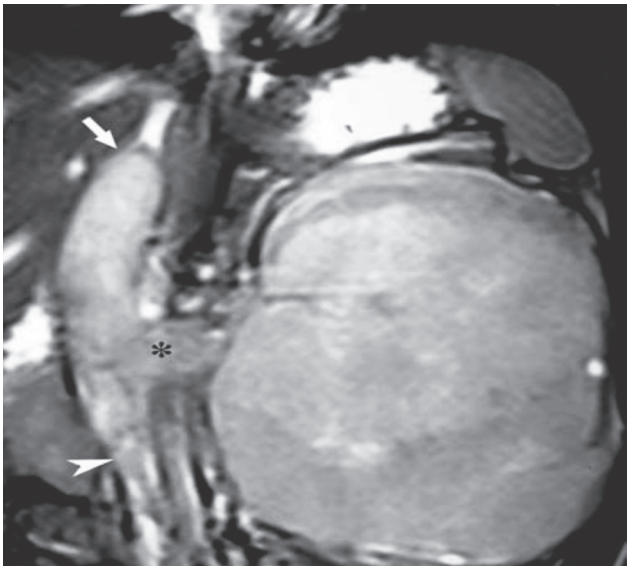

Renal cell carcinoma with tumor thrombus in the left renal vein and IVC. Coronal true FISP MR image shows a large, mildly hyperintense left renal mass with tumor thrombus distending the left renal vein (*) and suprarenal IVC (arrow). The cranial extent of the thrombus is well seen. Thrombus is also seen in the infrarenal IVC (arrowhead) but is not distending the lumen, findings that suggest bland thrombus.

FIGURE 16

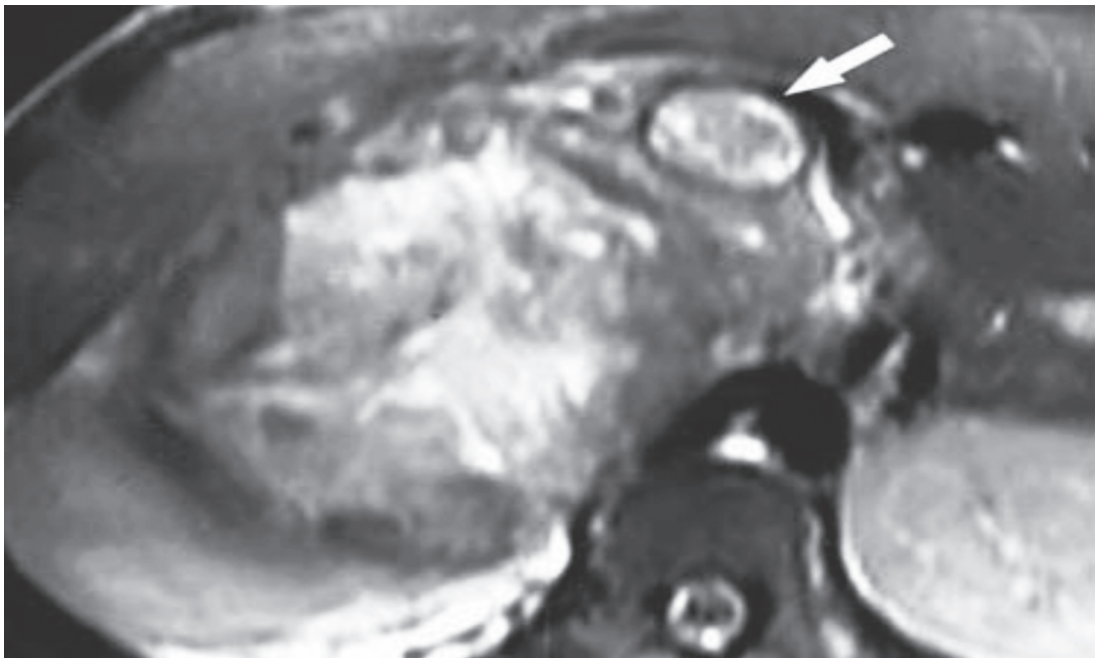

Adrenocortical carcinomawith IVC invasion. Axial T2-weighted MR image reveals a large, heterogeneous right adrenal mass with tumor thrombus and anteromedial displacement of the IVC (arrow).

FIGURE 17

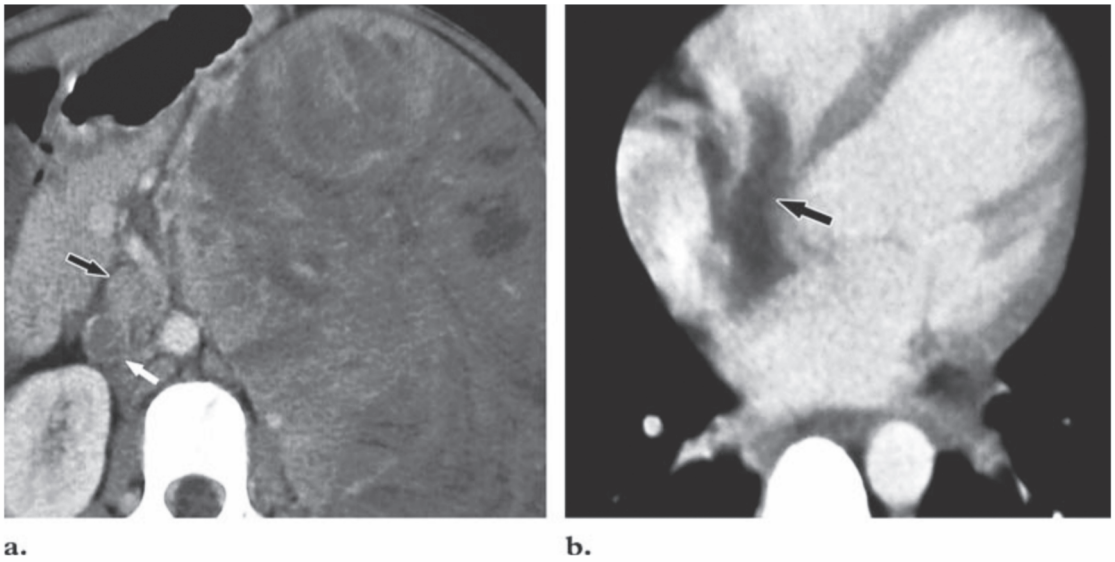

a. b.

Wilms' tumor with pulmonary embolism in a 3-year-old child. **(a)** Contrast-enhanced CT scan shows a large, heterogeneous left renal mass with tumor thrombus distending the renal vein (black arrow) and extending into the IVC (white arrow). **(b)** Contrast-enhanced CT scan shows cranial extension of the tumor into the right atrium and across the tricuspid valve (arrow). The patient died 2 days later, possibly due to massive embolism or tumor occlusion of the tricuspid valve orifice.

CASES 10 - 11

In blunt trauma patients, a flattened IVC at multiple levels is a strong indicator of hypovolemia or hypotension and may signify impending cardiovascular collapse (**FIG. 18**) (54). A flat IVC together with (a) a decreased caliber of the aorta, (b) marked diffuse bowel distention, (c) moderate to extensive hemoperitoneum, and (d) hyperenhancement of the bowel wall, kidneys, and pancreas constitutes the "hypoperfusion complex" seen at abdominal CT in blunt trauma patients (55). On the other hand, a CT finding of a flat IVC in patients without trauma usually does not signify hypotension, and only a few of these patients have evidence of hypovolemia (56).

Traumatic laceration of the IVC with herniation of intraabdominal fat or the presence of intravascular gas is a rare but striking finding in trauma victims (**FIG. 19**) (57,58).

FIGURE 18

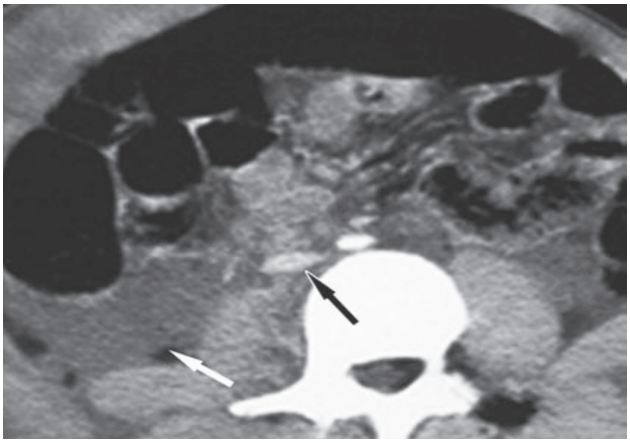

Flat IVC in a 47-year-old man who had been involved in a traffic accident. Contrast-enhanced CT scan reveals a collapsed IVC (black arrow). A collapsed aorta and gross hemoperitoneum (white arrow) are other indicators of hypoperfusion.

FIGURE 19

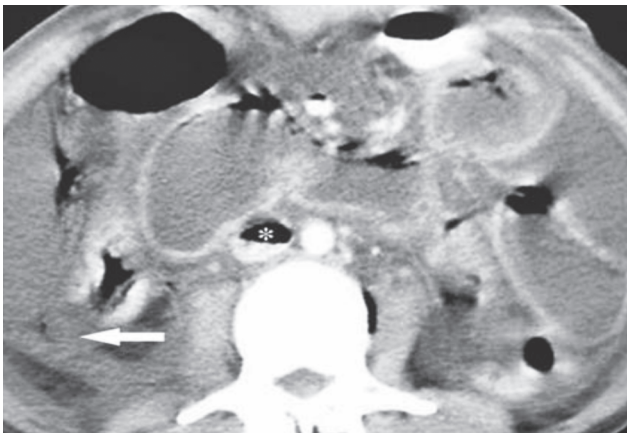

Posttraumatic air in the IVC in a 29-year-old man who had sustained blunt trauma to the abdomen. CT scan shows hemoperitoneum (arrow) with air forming a level in the IVC (*). Thepatient succumbed to his injuries.

CASE 12

Early enhancement of the IVC with dense undiluted contrast material can be due to reflux from the right atrium, aortocaval fistula, superior vena cava obstruction, or arteriovenous shunting in hypervascular liver tumors. Retrograde contrast enhancement of the IVC at a low injection rate (<3 mL/sec) is a highly specific although insensitive CT sign of right-sided heart diseases such as tricuspid regurgitation, pulmonary hypertension, and right ventricular systolic dysfunction (**FIG. 20**) (59). The predictive value of this sign diminishes at a higher injection rate (>3 mL/sec), since contrast material can then reflux from the right atrium into the IVC even in the absence of heart disease (**FIG. 21**) (59). On rare occasions, abdominal aortic aneurysm can erode into and form a fistulous communication with the IVC (prevalence, 0.2%–0.9%) (60). The rarity of this complication makes clinical diagnosis difficult unless the classic symptoms of abdominal pain, palpable aneurysm, and continuous bruit are present. Noninvasive imaging modalities including contrast-enhanced MR imaging and CT angiography are preferred over catheter angiography for the diagnosis of aortocaval fistula. Key imaging findings include the presence of an aortic aneurysm with early detection of dense contrast material in the dilated IVC (**FIG. 22**). The actual site of fistulous communication, represented by the loss of normal anatomic space between the aorta and the IVC, is often unclear at imaging (61). MR imaging has an advantage over CT in that many patients with aortocaval fistula have renal insufficiency, which discourages the use of iodinated contrast material (61). Timeofflight MR angiography also helps in making the diagnosis by revealing persistent flow in the despite the use of inferior saturation bands to eliminate venous inflow signal (61). Untreated aortocaval fistula is invariably fatal, but prompt diagnosis and surgical intervention can be life saving in many of

FIGURE 20

Retrograde contrast enhancement of the IVC in a 34-year-old woman with primarypulmonary hypertension and right-sided heart failure. Coronal maximum-intensity-projection image reveals dense undiluted contrast material in the IVC and hepatic veins. Note the dilatation of the central pulmonary arteries, right atrium, and IVC, all of which are manifestations of the patient's conditions. The filling defect in the IVC simulating thrombus (arrow) is artifactual and was not seen in the venous phase.

FIGURE 21

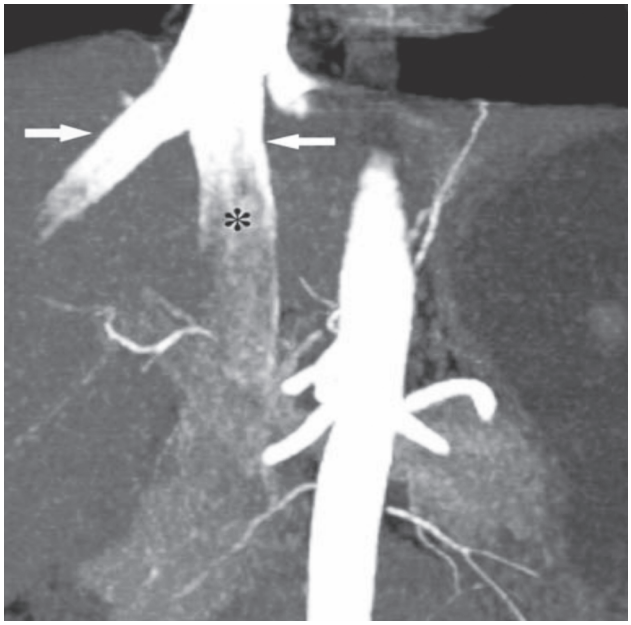

Retrograde contrast enhancement of the IVC in a 62-year-old man with normal cardiac function. Coronal maximum-intensity-projection reformatted image from CT angiographic data obtained at a high injection rate (4.5 mL/sec) shows the reflux of dense contrast material from the right atrium into the IVC and hepatic veins (arrows). Poor mixing between the unenhanced stream of blood in the IVC and the refluxed contrast material results in a filling defect (*) that may simulate thrombus, especially on axial images and in the absence of venous phase images, on which such artifactual lesions usually resolve.

FIGURE 22

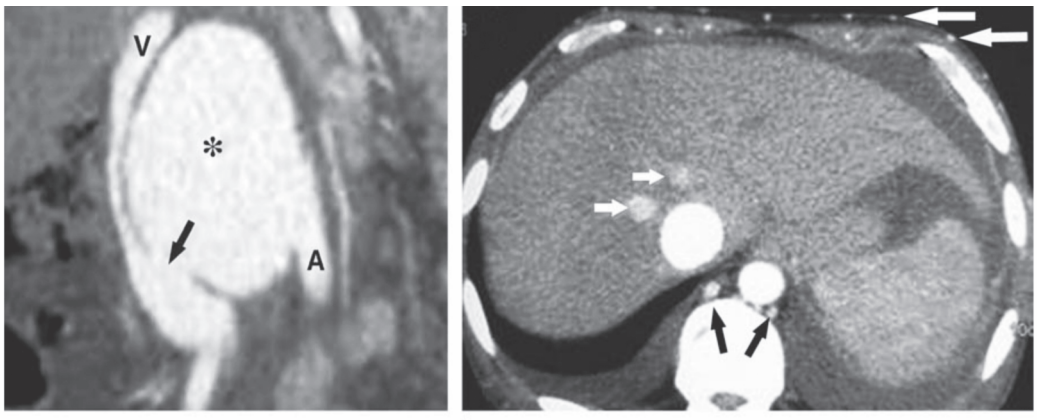

Aortocaval fistula in a 67-year-old man with rapid onset of dyspnea and pedal edema. **(a)** coronal reformatted CT image shows a large, infrarenal saccular aortic aneurysm (*) with aortocaval fistulous communication (arrow), resulting in simultaneous enhancement of the aorta **(A)** and IVC **(V)**. The infrarenal IVC is compressed and displaced by the aneurysm. **(b)** CT scan shows the reflux of dense contrast material into the hepatic veins (small white arrows), abdominal wall collateral vessels (large white arrows), and azygous-hemiazygous veins (black arrows). The intrahepatic IVC is dilated, and bilateral pleural effusion due to congestive heart failure is also seen.

these patients (62). The various collateral pathways seen in superior vena cava obstruction can result in early enhancement of the IVC. Collateral vessels following the azygous-hemiazygous and vertebral venous plexus routes drain directly into the IVC. Collateral vessels arising from the internal mammary and lateral thoracic veins drain first into the portal vein (cavoportal collateral route), resulting in abnormal liver enhancement, and then via the hepatic veins into the IVC (**FIG. 23**). Two cavoportal pathways have been descrive (63-65):

1. Internal mammary or lateral thoracic veins communicate with periumbilical collateral vessels that drain into the left portal vein. This pathway results in abnormal enhancement of the left hepatic lobe around the fissure for the ligamentum teres hepatis (**FIG. 23**).
2. The internal mammary vein is directly connected with the inferior phrenic vein that communicates with the intrahepatic portal venous system via its capsular branches, resulting in hyperenhancement of the subdiaphragmatic portion and bare area of the liver (**FIG. 23**). Hepatic venous invasion occurs in up to 26% of cases of HCC (66) and can also result in early enhancement of the IVC due to arteriovenous shunting (**FIG. 24**).

FIGURE 23

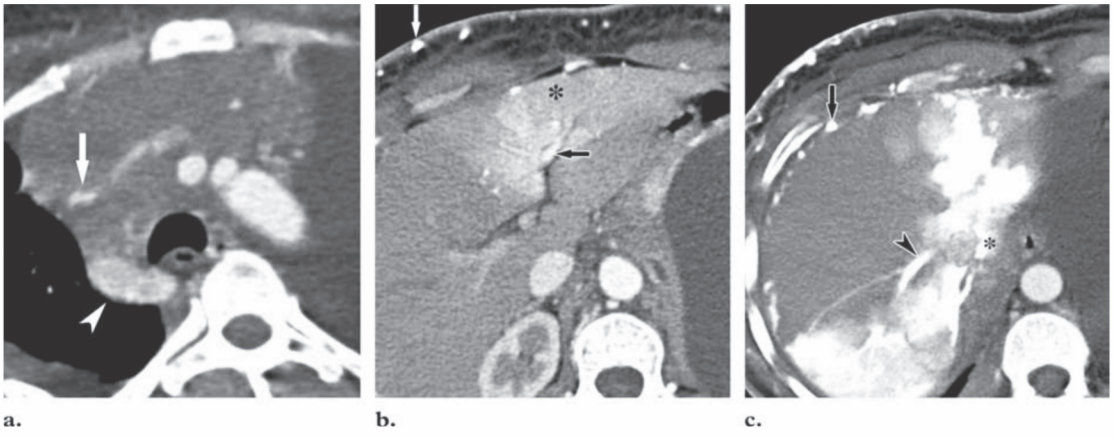

Cavoportal collateral pathways in a 53-year-old man with lung carcinoma. **(a)** Contrast-enhanced CT scan shows a large anterior mediastinal mass causing superior vena cava obstruction (arrow). The azygous vein is dilated (arrowhead). **(b)** Contrast-enhanced CT scan shows paraumbilical collateral vessels (white arrow) that comunicate with the left branch of the portal vein (black arrow), resulting in abnormal enhancement of the left hepatic lobe **(*)**. **(c)** Contrast-enhanced CT scan shows collateral vessels that connect with the subcapsular branches of the portal vein (arrow), resulting in abnormal enhancement of the left lobe and segment VII of the liver with early enhancement of the right hepatic vein (arrowhead) and IVC **(*)**.

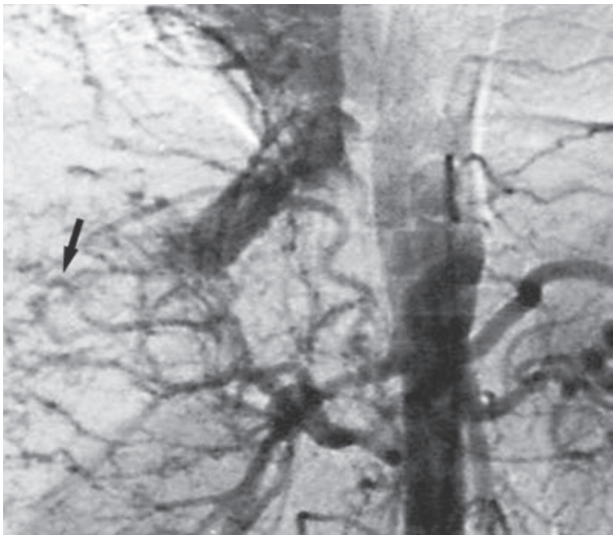

FIGURE 24

Arteriovenous shunting in HCC. Aortogram shows tumor neoangiogenesis (arrow) with early enhancement of the hepatic vein, IVC, and right atrium.

CASE 13

Pitfalls in imaging of the IVC are primarily due to a flow-related phenomenon or partial volume averaging artifact. A pseudo filling defect due to a flow-related phenomenon is most often seen the delayed postcontrast image, which is most reliable in distinguishing true thrombus from pseudothrombus (**FIG. 25**) (67). Other MR imaging sequences, including a balanced steadystate gradient-echo (true FISP) sequence and T1- and T2-weighted sequences, are also prone to flow-related artifactual signal in the IVC at the level of the renal veins (**FIG. 25**).

Pseudolipoma of the IVC is a partial volume averaging artifact caused by juxtacaval fat above the caudate lobe, rather than a true intraluminal lesion (**FIG. 26**) (51, 68). It has an association with cirrhosis, possibly because a shrunken right hepatic lobe not only tilts the IVC further but also accentuates peritava fat collection (69). The morphologic appearance of pseudolipoma may vary with inspiratory effort (68). As in pseudolipoma, partial volume averaging of pericaval fluid can mimic bland thrombus of the IVC at axial imaging (**FIG. 27**). ■

FIGURE 25

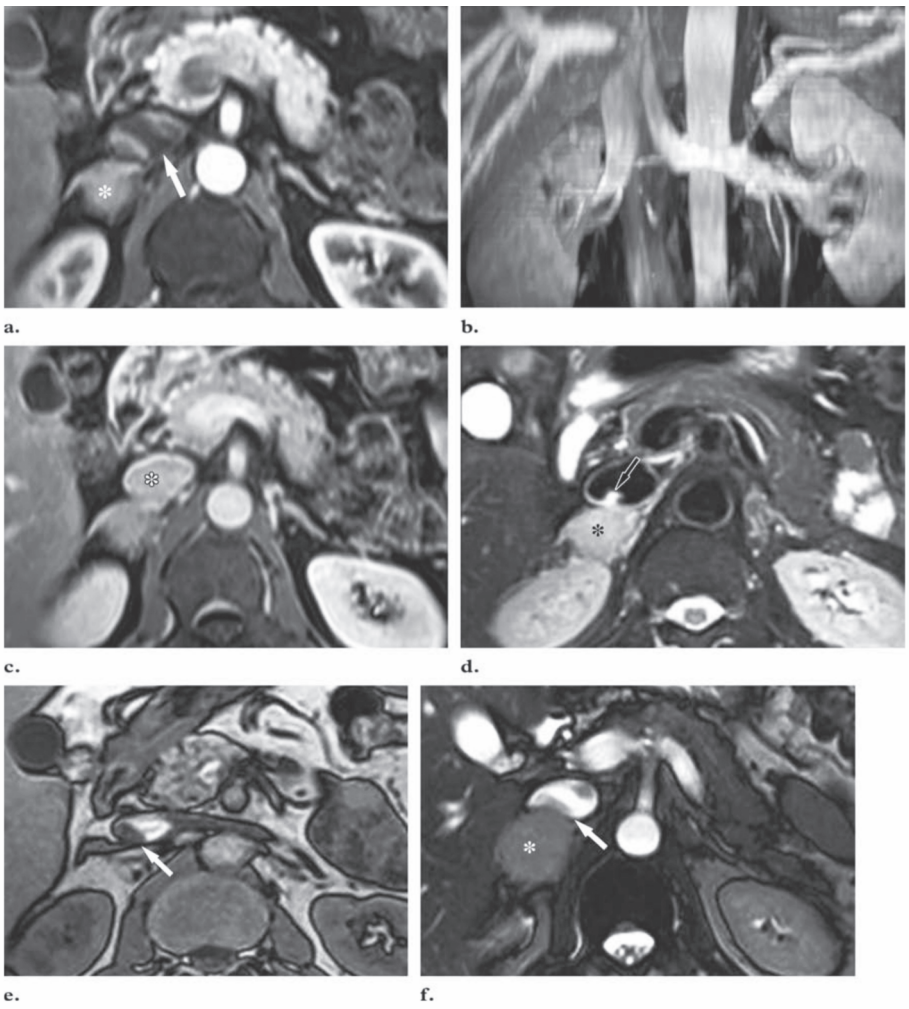

Pseudothrombus due to dense return from the renal veins in a patient with pheochromocytoma. (**a**) Gadolinium-enhanced corticomedullary phase T1-weighted MR image shows an apparent IVC filling defect. Arrow indicates pseudothrombus, * indicates pheochromocytoma. (**b, c**) Coronal reformatted image (**b**) shows dense return from the renal veins flowing along the IVC, and a nephrographic phase T1-weighted MR image (**c**) shows resolution of the filling defect, findings that confirm the artifactual nature of the lesion. * in **c** indicates pheochromocytoma. (**d–f**) Axial turbo spin-echo T2-weighted (**d**), gradient-echo T1-weighted (**e**), and true FISP (**f**) MR images show flow-related enhancement (arrow in **d**) and signal void due to phase dispersion (arrow in **e** and **f**) at the point where the two streams of blood with different velocities meet. * in d and f indicates pheochromocytoma.

FIGURE 26

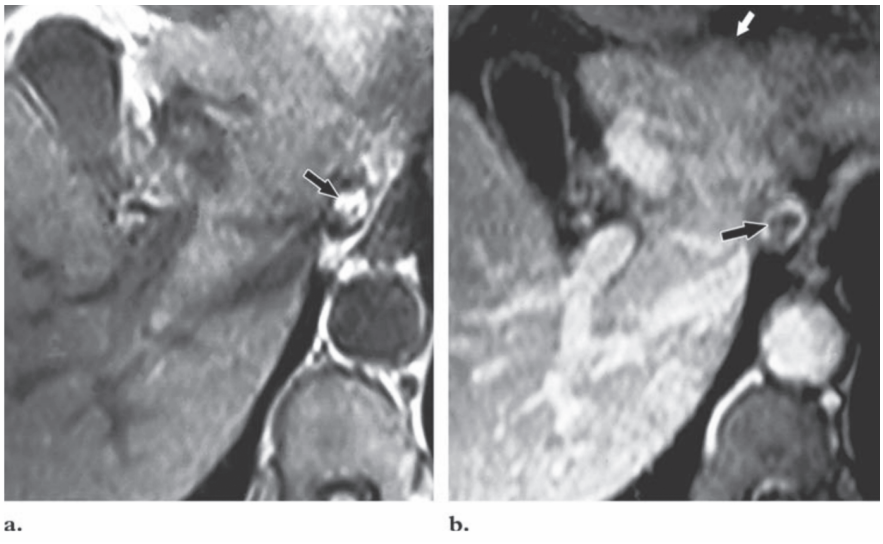

Pseudolipoma in a 46-year-old alcoholic patient with cirrhosis. **(a)** Axial T1-weighted MR image reveals a hyperintense lesion within the IVC (arrow), a finding that is suggestive of fat. **(b)** On a three-dimensional fat-suppressed volume-interpolated breathhold T1-weighted MR image, the lesion (black arrow) mimics a filling defect. Note that the shape of the lesion and its location within the IVC are different on the two images, a feature that is typical of pseudolipoma. A widened gallbladder fossa is noted, along with subtle liver surface nodularity (white arrow) due to underlying cirrhosis.

FIGURE 27

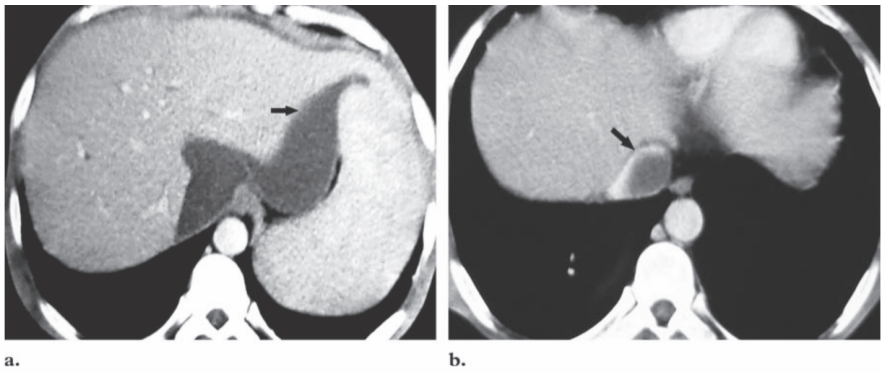

Pseudothrombus due to a pericaval fluid collection in a patient who had undergone cholecystectomy.
Contrast-enhanced CT scans show a biloma (arrow in **a**) and fluid around the IVC mimicking thrombus (arrow in **b**).

DISCUSSION

The IVC is host to a wide array of congenital anomalies and pathologic conditions. Imaging allows precise diagnosis of congenital variants and membranous obstruction of the intrahepatic IVC and is accurate in depicting the presence and extent of thrombus.
Other imaging findings such as flat IVC and early enhancement of the IVC are useful in limiting the differential diagnosis. Radiologists should be aware of the various pitfalls of IVC imaging and able to differentiate true from pseudo filling defects.

CONCLUSION

The Authors have explained cases report of patients with inferior vena cava anomalies.

REFERENCES

1. Phillips E. Embryology, normal anatomy, and anomalies. In: Ferris EJ, Hipona FA, Kahn PC, Phillips E, Shapiro JH, eds. Venography of the inferior vena cava and its branches. Baltimore, Md: Williams & Wilkins, 1969; 1–32.
2. Kellman GM, Alpern MB, Sandler MA, Craig BM. Computed tomography of the vena caval anomalies with embryological correlation. RadioGraphics 1988;8(3):533–556.
3. Bass JE, Redwine MD, Kramer LA, Huynh PT, Harris JH Jr. Spectrum of congenital anomalies of the inferior vena cava: cross-sectional imaging findings. RadioGraphics 2000;20:639–652.
4. Minniti S, Visentini S, Procacci C. Congenital anomalies of the venae cavae: embryological origin, imaging features and report of three new variants. Eur Radiol 2002;12:2040–2055.
5. Siegfried MS, Rochester D, Bernstein JR, Milner JW. Diagnosis of inferior vena cava anomalies by computerized tomography. Comput Radiol 1983;7:119–123.
6. Mathews R, Smith PA, Fishman EK, Marshall FF. Anomalies of the inferior vena cava and the renal veins: embryologic and surgical considerations. Urology 1999;53:873–880.
7. Evans JC, Earis J, Curtis J. Thrombosed double inferior vena cava mimicking paraaortic lymphadenopathy. Br J Radiol 2001;74:192–194.
8. Mano A, Tatsumi T, Sakai H, et al. A case of deep venous thrombosis with a double inferior vena cava effectively treated by suprarenal filter implantation. Jpn Heart J 2004;45:1063–1069.
9. Sartori MT, Zampieri P, Andres AL, Prandoni P, Motta R, Miotto D. Double vena cava filter insertion in congenital duplicated inferior vena cava: a case report and literature review. Haematologica 2006;91(6 suppl):ECR30.
10. Smith DC, Kohne RE, Taylor FC. Steel coil embolization supplementing filter placement in a patient with a duplicated inferior vena cava. J Vasc Interv Radiol 1992;3:577–580.
11. Talner LB, Reilly PHO, Wasserman NF. Specific causes of obstruction. In: Pollack HM, McClennan BL, eds. Clinical urography. 2nd ed. Philadelphia, Pa: Saunders, 2000; 1967–2136.
12. Bass JE, Redwine MD, Kramer LA, Harris JH Jr. Absence of the infrarenal IVC with preservation of the suprarenal segment as revealed by CT and MR venography. AJR Am J Roentgenol 1999;172:1610–1612.
13. Milner LB, Marchan R. Complete absence of the inferior vena cava presenting as a paraspinous mass. Thorax 1980;35:798–800.
14. d'Archambeau O, Verguts L, Myle J. Congenital absence of the inferior vena cava. J Belge Radiol 1990;73:516–517.
15. Monreal M, Lafoz E, Casals A, et al. Occult cancer in patients with deep venous thrombosis. Cancer 1991;67:541–545.
16. Dougherty MJ, Calligaro KD, DeLaurentis DA. Congenitally absent inferior vena cava presenting in adulthood with venous stasis and ulceration: a surgically treated case. J Vasc Surg 1996;23: 141–146.
17. Gibo M, Onitsuka H. Retroaortic left renal vein with renal vein hypertension causing hematuria. Clin Imaging 1998;22:422–424.
18. Schultz CL, Morrison S, Bryan PJ. Azygous continuation of the inferior vena cava: demonstration by NMR imaging. J Comput Assist Tomogr 1984;8:774–776.
19. Mazzucco A, Bortolotti U, Stellin G, Galucci V. Anomalies of the systemic venous return: a review. J Card Surg 1990;5:122–133.
20. Murray CP, Yoo SJ, Babyn PS. Congenital extrahepatic portosystemic shunts. Pediatr Radiol 2003;33:614–620.
21. Morgan G, Superina R. Congenital absence of the portal vein: two cases and a proposed

classification system for portosystemic vascular anomalies. J PediatrSurg 1994;29:1239–1241.
22. Yonemitsu H, Mori H, Kimura T, et al. Congenitalextrahepatic portocaval shunt associated with hepatic hyperplastic nodules in a patient with Dubin-Johnson syndrome. Abdom Imaging 2000;25:572–575.
23. Kakuno Y, Matsuki M, Kani H, Narabayashi I,Katayama H. Intrahepatic portosystemic venous shunt: Occurrence in a child patient without liver cirrhosis. Radiat Med 2004;22(3):195–197.
24. Hodkinson HJ, Kew MC. Membranous obstruction of the inferior vena cava and its causal relation to hepatocellular carcinoma. Liver Int 2006;26:1–7.
25. Okuda K, Kage M, Shrestha SM. Proposal of a new nomenclature for Budd-Chiari syndrome: hepatic vein thrombosis versus thrombosis of the inferior vena cava at its hepatic portion. Hepatology 1998;28:1191–1198.
26. Terabayashi H, Okuda K, Nomura F, Ohnishi K, Wong P. Transformation of the inferior vena caval thrombosis to membranous obstruction in a patient with lupus anticoagulant. Gastroenterology 1986;91:219–224.
27. Deutsch V, Rosenthal T, Adar R, Mozes M. Budd-Chiari syndrome: study of angiographic findings and remarks on etiology. Am J Roentgenol Radium Ther Nucl Med 1972;116:430–439.
28. Bargalló X, Gilabert R, Nicolau C, et al. Sonography of Budd-Chiari syndrome. AJR Am J Roentgenol 2006;187:W33–W41.
29. Sonin AH, Mazer MJ, Powers TA. Obstruction of the inferior vena cava: a multiple-modality demonstration of causes, manifestations, and collateral pathways. RadioGraphics 1992;12:309–322.
50. Hartman DS, Hayes WS, Choyke PL, Tibbetts GP. Leiomyosarcoma of the retroperitoneum and inferior vena cava: radiologic-pathologic correlation. RadioGraphics 1992;12:1203–1220.
51. Kaufman LB, Yeh BM, Joe BN, Qayyum A, Coakley F. Inferior vena cava filling defects on CT and MRI. AJR Am J Roentgenol 2005;185:717–726.
52. Svane S. Tumor thrombus of the inferior vena cava resulting from renal carcinoma: a report of 12 autopsied cases. Scand J Urol Nephrol 1969;3:245–256.
53. Didier D, Racle A, Etievent JP, Weill F. Tumor thrombus of the inferior vena cava secondary to malignant abdominal neoplasms: US and CT evaluation. Radiology 1987;162:83–89.
54. Jeffrey RB, Federle MP. The collapsed inferior vena cava: CT evidence of hypovolemia. AJR Am J Roentgenol 1988;150:431–432.
55. Taylor GA, Fallat ME, Eichelberger MR. Hypovolemic shock in children: abdominal CT manifestations. Radiology 1987;164: 479–481.
56. Eisenstat RS, Whitford AC, Lane MJ, Katz DS. The “flat cava” sign revisited: what is its significance in patients without trauma? AJR Am J Roentgenol 2002;178:21–25.
57. Brown MA, Hauschildt JP, Casola G, Gosink BB, Hoyt DB. Intravascular gas as an incidental finding at US after blunt abdominal trauma. Radiology 1999;210:405–408.
58. Sheafor DH, Foti TM, Vaslef SN, Nelson RC. Fat in the inferior vena cava associated with caval injury. AJR Am J Roentgenol 1998;171:181–182.
59. Yeh BM, Kurzman P, Foster E, Qayyum A, Joe B, Coakley F. Clinical relevance of retrograde inferior vena cava or hepatic vein opacification during contrast-enhanced CT. AJR Am J Roentgenol 2004; 183:1227–1232.
60. Alexander JJ, Imbembo AL. Aorto-vena cava fistula. Surgery 1989;105:1–12.
61. Schott EE 3rd, Fitzgerald SW, McCarthy WJ, Nemcek AA Jr, Sonin AH. Aortocaval fistula: diagnosis with MR angiography. AJR Am J Roentgenol 1997; 169:59–61.
62. Cohen LJ, Sukov RJ, Boswell W, Ashor G. Spontaneous aorto-caval fistula. Radiology 1981;138:357–359.
63. Dahan H, Arrive L, Cholley LM, Hir PL, Zins M, Tubiana JM. Cavoportal collateral

pathways in vena cava obstruction: imaging features. AJR Am J Roentgenol 1998;171: 1405–1411.

64. Baba Y, Miyazono N, Inoue H, et al. Altered flow dynamics of intravascular contrast material to the liver in superior vena cava syndrome: CT findings. Abdom Imaging 2000;25:146–150.
65. Cihangiroglu M, Lin BH, Dachman AH. Collateral pathways in superior vena caval obstruction as seen on CT. J Comput Assist Tomogr 2001;25(1):1–8.
66. Yu SC, Yeung DT, So NM. Imaging features of hepatocellular carcinoma. Clin Radiol 2004;59:145–156.
67. Pedrosa I, Morrin M, Oleaga L, Baptista J, Rofsky NM. Is true FISP imaging reliable in the evaluation of venous thrombosis? AJR Am J Roentgenol 2005;185:1632–1640.
68. Raju NL, Austin JH. Juxtacaval fat collection: mimic of lipoma in the subdiaphragmatic inferior vena cava. Radiology 2001;220:471–474.
69. Han BK, Im JG, Jung JW, Chung MJ, Yeon KM. Pericaval fat collection that mimics thrombosis of the inferior vena cava: demonstration with use of multi-directional reformation CT. Radiology 1997;203:105–108.

N° 12 ~ Supplemento al n° 41 Gennaio-Marzo 2019 del Trimestrale S.M.O.

Autorizzazione Trib. di Roma
n. 86/95 del 18/02/95